RSC Advances

ROYAL SOCIETY OF CHEMISTRY

www.rsc.org/advances

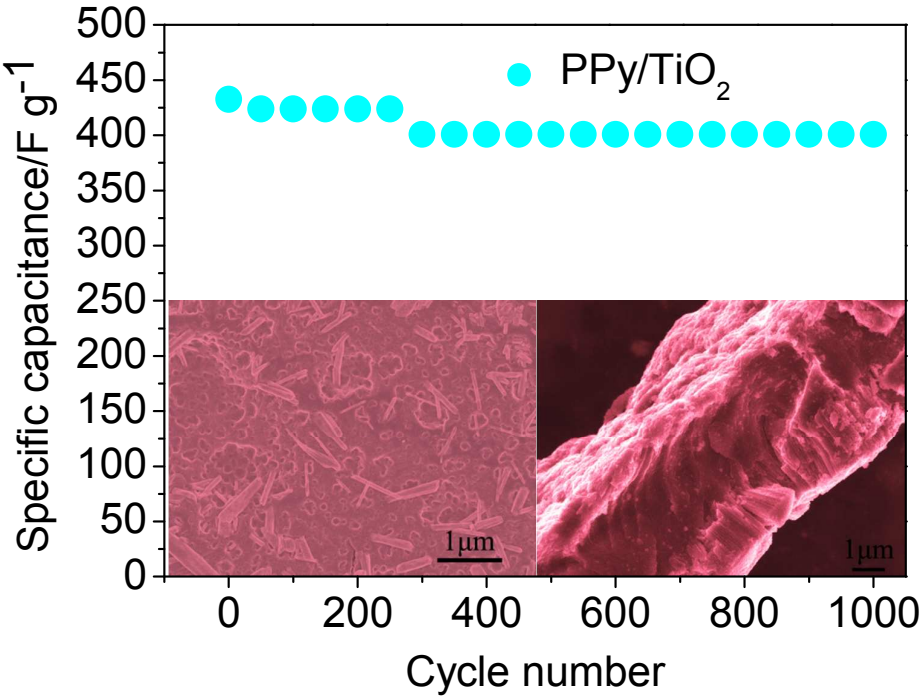

PPy film/TiO_2 nanotubes composite show enhanced cycling performance and higher specific capacity as anode materials for supercapacitor.

Cite this: DOI: 10.1039/c0xx00000x

www.rsc.org/xxxxxx

ARTICLE TYPE

PPy film/TiO_2 nanotubes composite with enhanced supercapacitive properties

Yan Gao,† Kun Ding,† Xin Xu* Yanzhou Wang and Demei Yu*

Department of Applied Chemistry, School of Science, Xi'anJiaotongUniversity, Xi'an 710049, China.
†Yan Gao and Kun Ding contributed equally to this work.
Email: xu.xin@stu.xjtu.edu.cn; dmyu@mail.xjtu.edu.cn

cReceived (in XXX, XXX) Xth XXXXXXXXX 20XX, Accepted Xth XXXXXXXXX 20XX
DOI: 10.1039/b000000x

In this paper, a film-on-tube PPy/TiO_2 composite composed of polypyrrole (PPy) and well-aligned TiO_2 nanotube array is reported. Pyrrole is polymerized on the top of TiO_2 nanotubes by a two-step anodic oxidation. The morphology and microstructure of these composites are characterized by scanning electron microscopy (SEM), transmission electron microscopy (TEM), Brunauer–Emmett–Teller (BET) and infrared spectroscopy (FT-IR). The electrochemical performance of the PPy/TiO_2 composite is determined by cyclic voltammetry and charge/discharge measurement. It indicates that these film-on-tube composites take advantage of the high electrochemical activity from TiO_2 and polypyrrole, the high electronic conductivity of PPy, and the large specific surface area of ordered TiO_2 nanotubes. These merits together with the elegant synergy between TiO_2 and PPy lead a good specific capacitance of 459 F/g at current density of 5A/g and excellent cycling stability with capacitance retention of 92.6% after 1000 charge/discharge cycles. The high capacitance as well as excellent cycling stability makes this film-on-tube composite promising for anode materials of supercapacitor.

1. Introduction

In recent years, rapidly increasing demands for energy storage of electronic devices and electric vehicles have attracted intense research on high performance electrode material. As one key energy storage device, supercapacitors have been playing an important role in many applications.[1] Based on the mechanism of charge storage, supercapacitors can be generally categorized into two types, electrochemical double-layer capacitors (EDLCs) and pseudocapacitors. For EDLCs, carbon-based materials are commonly used as electrodes due to their prominent long-term electrochemical stability as a result of high electrical conductivity and good chemical stability.[2, 3] However, the poor charge accumulation in electrical double layer confines the specific capacitances of EDLCs in a range of relatively small values. In pseudocapacitors, the charges are stored through some fast redox reactions of the anode materials, which make them exhibit much higher specific capacitance than the EDLCs.[4] However, pseudocapacitors are usually subjected to the poor electrical conductivity of electrode materials and the irreversibility of Faradaic reactions on electrode surface, which lead a gradual loss of capacitance during the charge-discharge processes. Up to now, there are two major approaches to solve these problems. One way is to develop nanostructured electrode materials with large effective area (nanotube,[5] nanosheet,[6] nanowire[7]), which exhibit higher specific capacitances compared to their bulk counterparts. Another approach is to improve the electrical conductivity of electrodes by combining them with highly conductive materials. For instance, Graphene materials as excellent electrical conductors have been widely used to form composites with metal oxide electrodes. Despite an increase of specific capacitances in Graphene-based composites such as MnO_2/Conjugated Polymer/Graphene[8] or MnO_2/Graphene Oxide,[9] the poor cycling stability of these composites limit their application.

Recently, various nanocomposites based on conducting polymers have been synthesized for energy storage.[10-12] Among them, Polypyrrole[13, 14] have attracted massive interests due to its electrochemical reversibility, environmental friendly, and ease preparation through chemical or electrochemical routes. Furthermore, the highly ordered TiO_2 nanotube arrays can be applied as a substrate material or high-performance electrode material owing to its high surface area and good chemical/electrochemical stability. It is important that the open-end nanotube structure offers an extremely large, solvated ion accessible surface area. Free-standing and through-hole TiO_2 nanotube arrays with controlled morphologies can be fully

fabricated by electrochemical method.[15, 16] However, the poor electrochemical activity and electrical conductivity of TiO_2 make it unqualified for supercapacitor application. To solve the above mentioned problems, some materials have been filled inside the TiO_2 nanotubes such as CdS, Cu, Fe[17-19] and conducting material.[20, 21] Recently, Nano-polypyrrole supercapacitor arrays have been prepared through Al_2O_3[22] and TiO_2 templates.[23] The organic−inorganic p-n heterostructures existed in these nanocomposites dramatically enhance the interface adhesion and charge transfer efficiency. With this speciality, these materials show great properties for sophisticated modern optical, electronic, and electrochemical devices including LPG sensors, supercapacitors and photovoltaic devices.[20, 23-25]

Herein, we use a two-step anodic oxidation[16] to achieve the TiO_2 nanotube arrays with uniform size, which are very suitable as templates for the polymerization of pyrrole on the top surface. PPy/TiO_2 film-on-tube composites were prepared through a conventional three-electrode system. This architecture can supply highly ordered structure to improve electron transfer effectiveness in a reversible redox reaction. The high specific surface area of nanotubes can also provide more sites for redox reaction between the active materials and electrolyte ions, consequently resulting in a high capacitance performance and specific capacity. It is also notable the synergism between TiO_2 nanotubes and PPy could effectively reduce the capacitance loss during charge-discharge process.

2. Experimental Section

Materials: Pyrrole (≥99.5%) was distilled before use, Ti foil (from Northwest Institute of Non-Ferrous Metals) was sliced into 3 cm × 3 cm × 0.01 cm. After polishing with abrasive paper, Ti was ultrasonicated (KQ-50B, from KUNS HAN Ultrasonic instrument Co.) in sequence (ethanol, acetone, deionized water) each for 5min for cleaning and then dried at room temperature before use.

All other reagents (analytical grade) were obtained from SHENTAI Tianjin Chemical Reagent Co. (China) and used as received without further purification.

2.1 Preparation of PPy/TiO_2film-on-tube composites

Fabrication of TiO_2 nanotube arrays: Well-aligned TiO_2 nanotube arrays were prepared by a two-electrode system with the Platinum as cathode and the commercial titanium foils as anode. The Ti samples were preanodized in a 0.5 wt % NH_4F ethylene glycol solution at 30 V for 6 h and then the achieved TiO_2 nanotube was removed by ultrasonication in 1 M HCl aqueous solution, leaving bowl-like foot-print on the surface. Then the samples were anodized for the second time in the electrolyte containing ethylene glycol, 1% hydrofluoric acid, and 0.5 wt % NH_4F at 30V for 4 h to get the well-aligned TiO_2 nanotubes. The samples were washed with deionized water and then dried at room temperature. The scheme is showed in Fig 1.

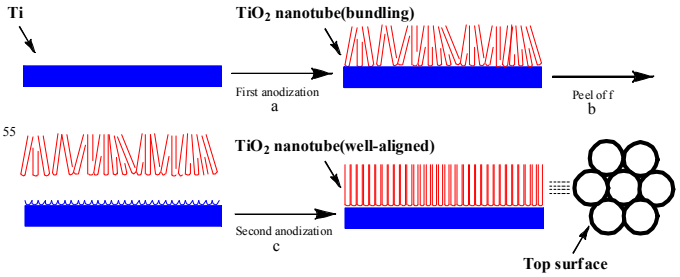

Fig. 1 The system of two-step anodic oxidation: a, First anodization; b, Peef off of TiO_2 nanotubes; c, Second anodization.

Fabrication of the PPy/TiO_2 film-on-tube composite: The PPy/TiO_2 composites were electrochemically prepared on electrochemical workstation by a conventional three-electrode system in 0.1 M $LiClO_4$ acetonitrile solution containing 0.2 M pyrrole at 0.8 V for 10 min. A standard three-electrode setup was used, with TiO_2 nanotubes prepared before as working electrode, Pt as the counter electrode and Ag as the reference electrode.

The PPy powder prepared by chemical method was used for comparison.[26]

2.2 Characterization

Surface morphologies of the materials were observed by field emission scanning electron microscopy (FESEM; JSM-6700F) and transmission electron microscopy (TEM; JEM-2100). To identify the chemical structure of pure PPy powder and PPy/TiO_2 film-on-tube composite, Infrared spectroscopy was performed by Fourier transform infrared spectrometer (Avator- FTIR-360) in the range of 400-4000cm^{-1}. The specific surface area and pore size distribution of the products were measured using a BET analyzer (ASAP 2020M).

2.3 Electrochemical measurements

Preparation of working electrode: The working electrode were prepared by mixing an active material (PPy/TiO_2 composites), a conductive agent (carbon blacks, super-P-Li), and a polymer binder (poly(vinylidenedifluoride), PVDF, Aldrich) in a 70:20:10 weight ratio and stirring at 25°C for 2 days. This mixture was then coated on the surface of aluminium foam (1cm×2cm×0.1cm) and dried at 140°C for 12h. The weight ratio of PPy and TiO_2 nanotubes in the composite is approximately 3.5 : 1.

The PPy-only and TiO_2-only electrode is made for comparation. The mass loading of the active materials is around 0.3 mg in the different electrodes.

Electrochemical measurements: The cyclic voltammetry (CV) measurement was carried out using an electrochemical workstation (CHI660D) in 1M H_2SO_4 electrolyte solution. A conventional three-electrode system was established where Pt foil serves as the counter electrode and a standard calomel electrode (SCE) as the reference electrode. The galvanostatic charge/discharge (GCD) measurements were conducted at the same condition of CV under a controlled current density and potential window range of 0-1V.

3. Results and discussion

The scanning electron microscopy and transmission electron microscopy was used to characterize microstructure of TiO_2 nanotubes arrays and PPy/TiO_2 composite. SEM images of bare TiO_2 nanotube arrays are shown in Fig. 2. It can be seen that the surfaces through only one-step anodization have many defects and debris covering the top of the nanotubes (Fig. 2a and b). Bundling and sealing on the top surface are also very serious which is mainly induced by the over-etching of the top parts. Sealing and bundling renders the ion hard to get through the TiO_2 nanotubes, which may significantly decrease the transfer efficiency. Yet from Fig. 2c and d it indicates that each nanotube is open and has its own wall. No sealing and bundling defects were brought about with the perfect alignment of nanotube surfaces. Transmission electron microscopy (TEM) images (inset of Fig. 2c) further indicate that the inner diameter of TiO_2 nanotubes is around 50 nm. The total length is approximate 2-3 µm (Fig. 2d). Highly ordered and vertically oriented TiO_2 nanotubes array offers high surface area of nanotube walls without a concomitant decrease in geometric and structural order. This well-aligned nanotube structure is beneficial to deposit polypyrrole on the top and facilitate charge transfer. The Brunauer–Emmett–Teller (BET) specific surface area of TiO_2 nanotubes is about 39 m^2/g (Fig.3a), and the plot (Fig. 3b) shows that most pores

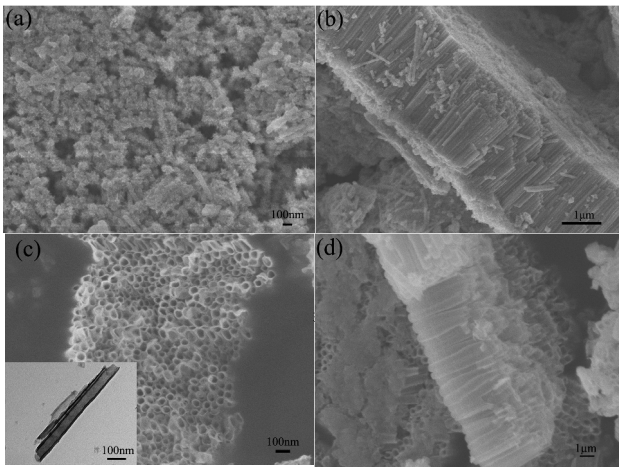

Fig. 2 SEM images of top surface view and cross-section view of TiO_2 nanotube by one-step anodization (a, b) and two-step anodization (c, d). The inset shows the morphology of the single TiO_2 nanotube.

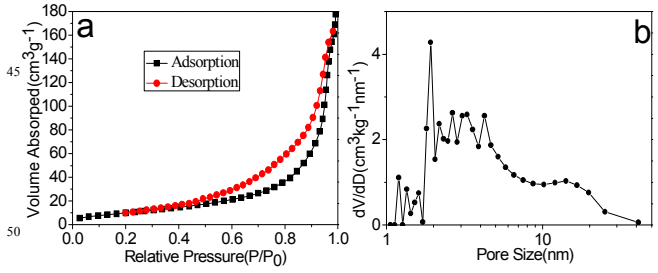

Fig. 3 (a) Nitrogen adsorption/desorption isotherm of the TiO_2 nanotubes; (b) The pore size distribution calculated using the BJH method from the desorption curve.

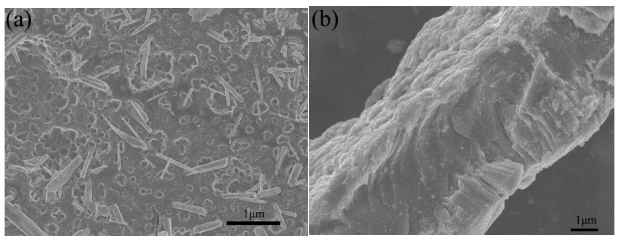

Fig.4 SEM images of top surface view (a) and cross-section view (b) of PPy/TiO_2 film-on-tube composite.

are in the mesoporous range with a peak between 2-12 nm.

SEM images of PPy/TiO_2 composite are shown in Fig. 4. It shows that pyrrole is polymerized on the top of TiO_2 nanotubes to form a film-on-tube structure. It can also be seen that some PPy nanowires reach out and are inclined to bond together. The total length of this film-on-tube composite is 3-4 µm, which is about two time of the length of bare TiO_2 nanotubes. The controlled electropolymerization process becomes a feasible approach to polymerize PPy on the top of TiO_2 nanotubes to form film-on-tube composite. It is believed that such an ordered and coaxial nanotube structure contributes highly effective interface area to provide more sites for redox reaction between the active materials and electrolyte ions, consequently enhancing the electrochemical capacitance performance.

Fig. 5 shows the FT-IR spectra of different samples. The main characteristic peaks of PPy can be assigned as follows: The appearance of a band at 3446.36 cm^{-1} shows the characteristic of N-H absorption peak. The band at 1539 cm^{-1} is due to the symmetric and antisymmetric ring-stretching modes.[27] Strong peaks near 1159 cm^{-1} indicate the doping state of polypyrrole. The peaks at 1036 and 1297 cm^{-1} are attributed to C-H deformation vibrations and C-N stretching vibrations, respectively, and is well consistent with the reported bands.[28] These bands also appear in the FTIR spectrum for PPy/TiO_2 sample, following curve (3427, 1632, 1088, 992 cm^{-1}), implying the formation of PPy backbone chains. The absorption bands at around 470 cm^{-1} are attributed to Ti-O stretching and Ti-O-Ti bridging stretching modes. However, a N-H bond absorption peak red shift as well as C = C bond absorption peak blue shift happen in the spectrum of the composite, which might due to the low concentration of PPy as well as the possible interplay of PPy with TiO_2 in the composites.

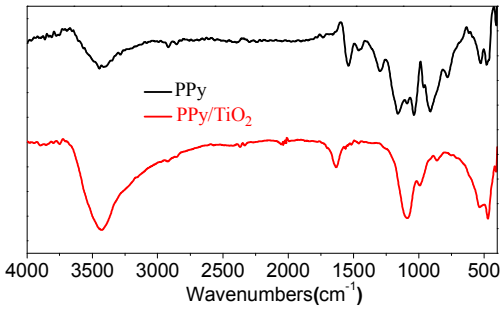

Fig. 5 FT-IR spectra of different samples.

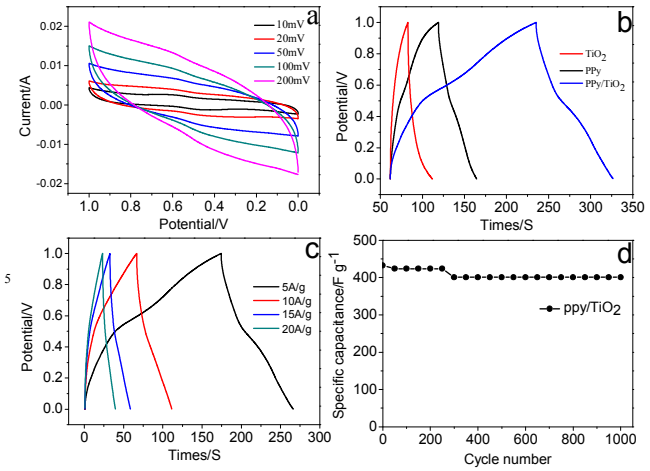

Fig. 6 (a) Cyclic voltammetry curves of PPy/TiO_2 composite at scan rate from 10 mV/s to 200 mV/s; (b) Galvanostatic charge/discharge curves of PPy,TiO_2 and PPy/TiO_2 composites at current density of 5A/g; (c) Galvanostatic charge/discharge curves of PPy/TiO_2 composites at current density of 5, 10, 15 and 20 A/g; (d) Cycling stability of PPy/TiO_2 composites.After 1000 cycles, 92.6% capacitance can still be retained. All above test in 1M H_2SO_4 electrolyte solution.

Fig. 6a shows the cyclic voltammetry (CV) curves of the as-obtained PPy/TiO_2 composite measured in the electrolyte of 1M H_2SO_4 at scan rates of 10, 20, 50, 100, 200 mV/s. It reveals an oblique and narrow CV loop, reflecting the pseudocapacitive characteristic of the conducting polymers. When the scan rates are below 50mV/s, a pair of broad oxidation and reduction current peaks is clearly discovered, which is contributed to the redox process of PPy in the composite. Fig. 6b shows galvanostatic charge-discharge curves of the TiO_2, PPy and PPy/TiO_2 composite at current density of 10 A/g. The gravimetric specific capacitance (C_m) is calculated using the following equation:

$$C_m = I \times \Delta t/(\Delta V \times m)$$

where C_m (F/g) is the specific capacitance, I (A) is the discharge current, Δt (s) is the discharge time, ΔV (V) is the potential change during discharge, m (g) is the mass of the active material in each electrode. Therefore, the specific capacitances are calculated to be 148, 227.5 and 459 F/g corresponding to the TiO_2, PPy and PPy/TiO_2 composite, respectively（at current density of 5 A/g）. These results show that these film-on-tube PPy/TiO_2 ncomposites possess higher electrochemical performance than the TiO_2 nanotubes and chemically-fabricated PPy-only materials. In addition, the specific capacitances of the PPy/TiO_2 composite at different current densities are also measured subsequently with the results shown in Fig. 6c. The values are also calculated to be 459, 432.6, 387, 331 F/g at current densities of 5, 10, 15, 20 A/g.

To make a further study, the cycling stability of PPy/TiO_2 composite is displayed in Fig. 6d. When the charge–discharge current density is 10 A/g, the specific capacitance is around 432.6 F/g in the first cycle, and it slightly decreases to 424 F/g in the course of first fifty cycles. We believe that the capacitance decay during the 200-300 charge/discharge cycles is related to the rapid swelling/shrinkage of the polymer backbone during the charge-discharge process, resulting in the deterioration of the original structure of PPy and lead to the formation of cracks in the electrode film. As a result, the transmission of electric charges is restrained, which cause the decline of the capacitance. [29, 30] After 300 cycles, the PPy chains tend to stabilize and it gradually decreases to 400 F/g after 1000 cycles, resulting in an overall capacitance loss of 7.4%. The exceptional cycling stability of the supercapacitor is attributed to the stability of the individual electrodes: the highly ordered PPy film with ultra-small thickness, which is benefit for the electrochemical performance. The TiO_2 nanotubes can also be regarded as the skeleton of the hybrid structures, thus the electrode materials' large volume change accompanying the charge-discharge process can be buffered, which brings stable cycling performance. [31]

4. Conclusions

In this paper, PPy/TiO_2 film-on-tube composites were fabricated by polymizing conducting polypyrrole on the top of well-aligned TiO_2 nanotubes arrays through a facile electropolymerization synthesis route. Morphological analysis confirms the polypyrroles were electropolymerized on the top of TiO_2 nanotubes, forming a highly ordered organic-inorganic structure. Electrochemical measurements show that TiO_2 nanotubes substrate obviously improves the electronic conductivity of the PPy/TiO_2 film-on-tube composite, thus facilitating the fast kinetics of electrochemical reaction and leading to enhanced rate capability. Hence, the specific capacitance of PPy/TiO_2 film-on-tube composite is 459 F/g at current density of 5 A/g which is way better than PPy-only (227 F/g) devices. More importantly, these composites shows an outstanding cycling stability (92.6% capacitance retention after 1000 cycles) that probably due to the synergetic contribution from TiO_2 nanotubes and conductive PPy. Our work not only presents the possibility to design TiO_2 nanotubes into a promising pseudocapacitive material, but also opens up an affordable general approach to devise composite electrode architectures for solar cells and energy storage devices.

Acknowledgements

The work was supported by NSFC Major Research Plan on Nanomanufacturing (Grant No. 91323303).

References

1. A. Ghicov and P. Schmuki, *Chem. Commun.*, 2009, 2791-2808.
2. A. Izadi-Najafabadi, T. Yamada, D. N. Futaba, M. Yudasaka, H. Takagi, H. Hatori, S. Iijima and K. Hata, *ACS Nano*, 2011, **5**, 811-819.
3. A. Izadi‐Najafabadi, S. Yasuda, K. Kobashi, T. Yamada, D. N. Futaba, H. Hatori, M. Yumura, S. Iijima and K. Hata, *Adv. Mater.*, 2010, **22**, E235-E241.
4. X. Lu, G. Wang, T. Zhai, M. Yu, J. Gan, Y. Tong and Y. Li, *Nano lett.*, 2012, **12**, 1690-1696.

5. C.-C. Hu, K.-H. Chang, M.-C. Lin and Y.-T. Wu, *Nano lett.*, 2006, **6**, 2690-2695.
6. X. Xia, J. Tu, Y. Zhang, Y. Mai, X. Wang, C. Gu and X. Zhao, *J. Phys. Chem. C*, 2011, **115**, 22662-22668.
7. X. Lu, T. Zhai, X. Zhang, Y. Shen, L. Yuan, B. Hu, L. Gong, J. Chen, Y. Gao and J. Zhou, *Adv. Mater.*, 2012, **24**, 938-944.
8. C. X. Guo, M. Wang, T. Chen, X. W. Lou and C. M. Li, *Adv. Energy Mater.*, 2011, **1**, 736-741.
9. A. F. Sumboja, C. Y. Wang, X. Lee, P. S., *Adv. Mater.*, 2013, **25**, 2809-2815.
10. X. Xia, D. Chao, X. Qi, Q. Xiong, Y. Zhang, J. Tu, H. Zhang and H. J. Fan, *Nano lett.*, 2013, **13**, 4562-4568.
11. F. Wang, S. Xiao, Y. Hou, C. Hu, L. Liu and Y. Wu, *RSC. Adv.*, 2013, **3**, 13059–13084.
12. J. Zhu, M. Chen, Q. He, L. Shao, S. Wei and Z. Guo, *RSC. Adv.*, 2013, **3**, 22790-22824.
13. Q. Qu, Y. Zhu, X. Gao and Y. Wu, *Adv. Energy Mater.*, 2012, **2**, 950-955.
14. W. Tang, L. Liu, Y. Zhu, H. Sun, Y. Wu and K. Zhu, *Energy& Environ. Sci*, 2012, **5**, 6909-6913.
15. D. Wang and L. Liu, *Chem. Mater.*, 2010, **22**, 6656-6664.
16. D. Wang, B. Yu, C. Wang, F. Zhou and W. Liu, *Adv. Mater.*, 2009, **21**, 1964-1967.
17. D. Wang, Y. Liu, C. Wang, F. Zhou and W. Liu, *ACS Nano*, 2009, **3**, 1249-1257.
18. J. M. M. Andrei Ghicov, *Nano lett.*, 2006, **6**, 1080-1082.
19. J. M. Macak, B. G. Gong, M. Hueppe and P. Schmuki, *Adv. Mater*, 2007, **19**, 3027-3031.
20. D. Wang, Q. Ye, B. Yu and F. Zhou, *J. Mater. Chem.*, 2010, **20**, 6910.
21. F. D. Sudip Barman, and Richard L. McCreery, *J. Am. Chem. Soc.*, 2008, **130**, 11073-11081
22. L. Liu, Y. Zhao, Q. Zhou, H. Xu, C. Zhao and Z. Jiang, *J. Solid State Electr.*, 2005, **11**, 32-37.
23. M. Yu, Y. Zeng, C. Zhang, X. Lu, C. Zeng, C. Yao, Y. Yang and Y. Tong, *Nanoscale*, 2013, **5**, 10806-10810.
24. T. Jiang, Z. Wang, Z. Li, W. Wang, X. Xu, X. Liu, J. Wang and C. Wang, *J. Mater. Chem. C*, 2013, **1**, 3017-3025.
25. R. N. Bulakhe, S. V. Patil, P. R. Deshmukh, N. M. Shinde and C. D. Lokhande, *Sensors and Actuat. B: Chem.*, 2013, **181**, 417-423.
26. J. Stejskal, M. Omastová, S. Fedorova, J. Prokeš and M. Trchová, *Polymer*, 2003, **44**, 1353-1358.
27. G. Cho, B. M. Fung, D. T. Glatzhofer, J.-S. Lee and Y.-G. Shul, *Langmuir*, 2001, **17**, 456-461.
28. B. Guo, Q. Kong, Y. Zhu, Y. Mao, Z. Wang, M. Wan and L. Chen, *Chem.*, 2011, **17**, 14878-14884.
29. P. Si, S. Ding, X. Lou and D. Kim, *RSC Adv.*, 2011, **1**, 1271-1278
30. Y. Zhou, Q. L. Bao, L. A. L. Tang, Y. L. Zhong and K. P. Loh, *Chem. Mater.*, 2009, 21, 2950-2956.
31. X. Xu, Z. Fan, S. Ding, D. Yu and Y. Du. *Nanoscale*, 2014, **6**, 5245-5250.